Digest Journal of Nanomaterials and Biostructures Vol. 11, No. 1, January - March 2016, p. 23 - 32

PHYSICAL AND MECHANICAL PROPERTIES OF Ni-Al NANOALLOYS USING MOLECULAR DYNAMICS SIMULATION

T. H. FANG[a], W. J. CHANG[b*], P. C. CHENG[a]
[a]*Department of Mechanical Engineering, National Kaohsiung University of Applied Sciences, Kaohsiung 807, Taiwan*
[b]*Department of Mechanical Engineering, Kun Shan University, Tainan 710, Taiwan*

Using a molecular-dynamics simulation with a tight-binding potential, we studied the physical and mechanical properties of Ni–Al nanoalloys with different compositions during quenching. The results showed that the radial distribution function of the monocrystalline Ni–Al nanoalloy exhibited higher peaks and deeper valleys than those of the amorphous one. The height of the first peak of the function slightly decreased as the equilibrium temperature increased. The phase transformation from monocrystalline to amorphous was accompanied by a volume expansion of approximately 1.5% after quenching. In addition, the area reduction of the monocrystalline Ni–Al nanoalloy with a Ni:Al ratio of 5:5 was more uniform than that of the amorphous one in the neck region.

(Received November 5, 2015; Accepted January 6, 2016)

Keywords: Ni-Al nanoalloy; molecular dynamics; mechanical property;
Thermal expansion coefficient.

1. Introduction

Ni–Al alloys have attracted significant research interest because of their low densities, high melting points, and excellent corrosion resistances at elevated temperatures [1–3]. These alloys have been used in high-temperature dies and molds, jet aircraft engines, and cutting tools [4–5].

With the development of nanotechnology, nanostructured Ni–Al alloys are promising materials for applications in micro-/nano-electro-mechanical systems. The characteristics of Ni–Al nanoalloy materials have been extensively studied in the past few years. One of the major reasons for interest in nanoalloy materials is that their physical and chemical properties can be changed by varying their compositions and sizes. Molecular dynamics (MD) simulations [6–10] have been very effective at simulating the material characteristics of Ni–Al nanoalloys because of the rapid development of computer technology in recent years [11–16]. For example, Ozgen and Adiguzel [12] investigated the thermoelastic phase transformation in a Ni–Al alloy using MD simulation with a Lennard–Jones potential.

Kazanc and Tatar [14] studied the effects of applied pressure on the transformation temperature, enthalpy, entropy, and elastic energy of a nanoalloy system using the embedded atom method (EAM) based on many-body interactions. They found that the transformation temperature increased with applied pressure, whereas the enthalpy, entropy, and elastic energy decreased. Levchenko et al. [15] studied the surface segregation, density, surface energy, and self-diffusion in a liquid Ni–Al alloy cooled down from its melting temperature. They used MD simulation with an

---

[*] Corresponding author: changwj@mail.ksu.edu.tw

EAM potential and found that the degree of segregation increased with undercooling and that Al had a lower surface energy than Ni.

Most of the above-mentioned literature focuses on the structural characteristics of Ni–Al nanoalloys, while their mechanical properties have been investigated in only few studies [17]. In the research described herein, the effects of temperature and composition on the physical and mechanical properties of Ni–Al nanoalloys were studied using MD simulation with a many-body tight-binding (TB) potential [17–18].

2. Methodology

MD simulations were performed to study the effects of the quenching process on the mechanical properties of Ni–Al nanoalloys with different compositions. The initial configuration of the system in a monocrystalline state at 300 K was obtained from a random distribution, as shown in Fig. 1. The Ni–Al nanoalloy with a Ni:Al ratio of 5:5 experienced a phase transformation from monocrystalline to amorphous after heating, holding, and cooling during the quenching process. The amorphous structure was similar to that of liquid nanoalloy. The total number of atoms in two components was 20250, and a time step of 1 fs was used in the simulations.

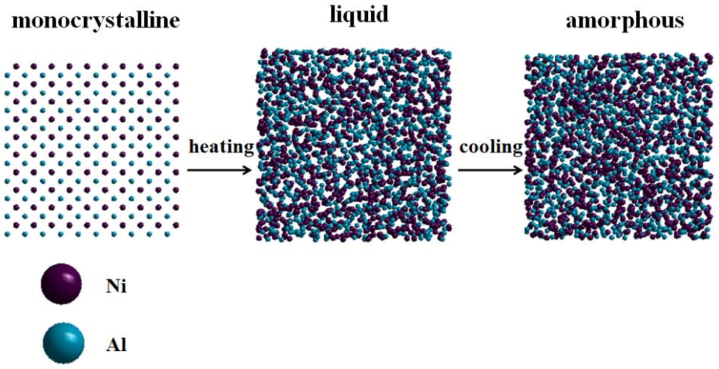

Fig. 1. Phase transformation of Ni-Al nanoalloy structure during thermal treatments.

In this research, a many-body TB potential [13] was used to simulate atomic interactions. The parameter values used in the simulation, namely Ni–Al, Ni–Ni, and Al–Al, are listed in Table 1 [13]. The TB potential can be expressed as [13]

$$E = \sum_i (E_R^i + E_B^i) \tag{1}$$

where E_R^i and E_B^i denote the repulsive energy and bond-structure energy of atom i, respectively, and can be expressed as

$$E_R^i = \sum_j A e^{-p\left[r_{ij}/r_0 - 1 \right]} \tag{2}$$

and

$$E_B^i = -\left\{ \sum_j \xi^2 e^{-2q\left[r_{ij}/r_0 - 1 \right]} \right\} \tag{3}$$

where A and p are parameters determined from the experimental data and are related to the cohesive energy and compressibility of the bulk metal, respectively; r_0 is the first-neighbor distance; r_{ij} is the distance between atoms *i* and *j*; ξ is an effective hopping integral; and *q* describes its dependence on the relative interatomic distance.

Table 1. Tight-binding potential parameters used in the MD simulation [13].

	A (eV)	**ξ (eV)**	**r_0 (nm)**	**p**	**q**
Ni-Al	0.0678	1.186	2.677	12.805	1.852
Al-Al	0.1221	1.316	2.864	8.612	2.516
Ni-Ni	0.0376	1.070	2.491	16.999	1.189

3. Results and Discussion

3.1 Effects of quenching process

The step-function temperature profile obtained by heating, holding, and cooling during the quenching period is shown in Fig. 2. The quenching process was performed by heating to 1500 K at a rate of 10 K/ps and then holding the temperature at 1500 K for 100 ps. The holding temperature of 1500 K ensured that the monocrystalline alloys transformed to the amorphous liquid state. The simulated alloys were then cooled down to the room temperature of 300 K at cooling rates of 5 K/ps, 10 K/ps, 20 K/ps, and 100 K/ps.

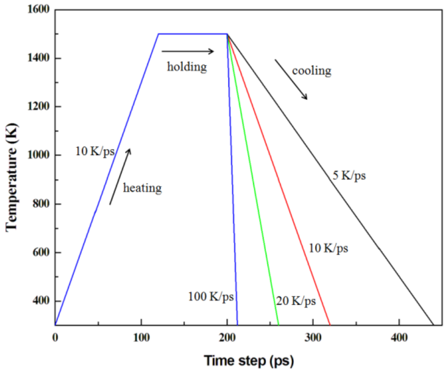

Fig. 2. The temperature-time history for quenching of Ni-Al nanoalloy during heating, holding and cooling periods at different cooling rates

It is well known that the volume of a material is related to its temperature and thermal expansion coefficient. The volume of a Ni–Al nanoalloy with a ratio of 5:5 was measured during heating at a rate of 10 K/ps, holding, and cooling at different rates, as shown in Fig. 3. During the heating process, the volume increases with increasing temperature. The maximum volume occurs during the holding period. After holding, the volume of the nanoalloy contracts during the cooling process. The rate of change of the volume of an alloy depends on its thermal expansion coefficient. The thermal expansion coefficient is the thermal property that relates changes in temperature to changes in spatial dimensions and is determined by the atomic lattice and metallic bonding at an atomistic scale. During the heating process, the rate of change of the volume becomes large after the melting temperature is reached, indicating that the thermal expansion coefficient of the nanoalloy in the liquid state is greater than that in the solid phase. The simulated melting point of the Ni–Al nanoalloy was about 1030 K. In addition, it can be seen that the volume of the Ni–Al amorphous nanoalloy was approximately 1.5% larger than that of the monocrystalline alloy at room temperature.

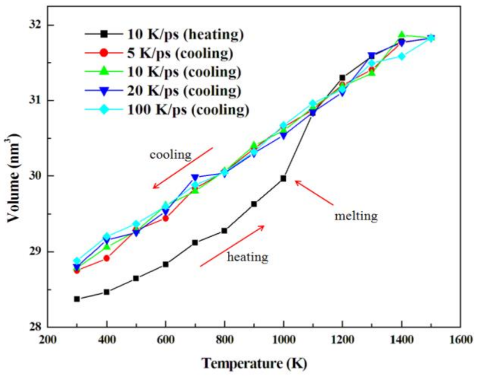

Fig. 3. The volume of a Ni-Al nanoalloy with a ratio of 5:5 as a function of temperature at different cooling rates. The simulated melting point of the Ni-Al alloy is about 1030 K

Fig. 4 illustrates the relationship between the radial distribution function and the radial separation for monocrystalline and amorphous Ni–Al nanoalloys with ratios of 5:5, at 300 K. The location of the first peak in the radial distribution function denotes the nearest interatomic distance, which is estimated to be 0.25 nm at 300 K. The radial distribution function of the monocrystalline state exhibits higher peaks and deeper valleys than that of the amorphous one due to the density effect. This effect can be explained by Fig. 3, which indicates that the density of the Ni–Al monocrystalline state is greater than that of the amorphous one.

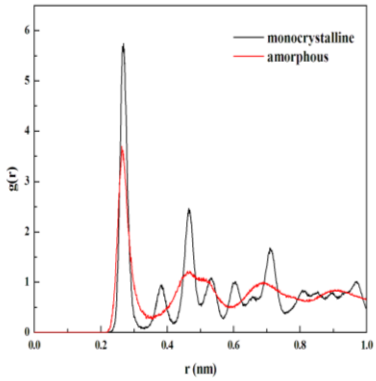

Fig. 4. Comparison of radial distribution functions for monocrystalline and amorphous Ni-Al nanoalloys with a ratio of 5:5 at 300 K

3.2 Effects of composition

To study effects of composition on the mechanical properties of amorphous Ni–Al nanoalloys, three alloys were simulated, with ratios of 3:7, 4:6, and 5:5. Fig. 5 shows the configurations of monocrystalline and amorphous Ni–Al nanoalloys at 300 K. The lengths, widths, and thicknesses of the Ni–Al nanoalloys were 14.2 nm, 4.5 nm, and 4.5 nm, respectively. The atoms of the upper and lower layers (about 1.1 nm thick) were fixed, and the others were variable. By increasing the displacement of atoms in the length direction, tensile loading was applied to the boundary atoms at a rate of 30 m/s. The temperature employed in the calculations was 300 K, and the influence of thermal vibration was neglected.

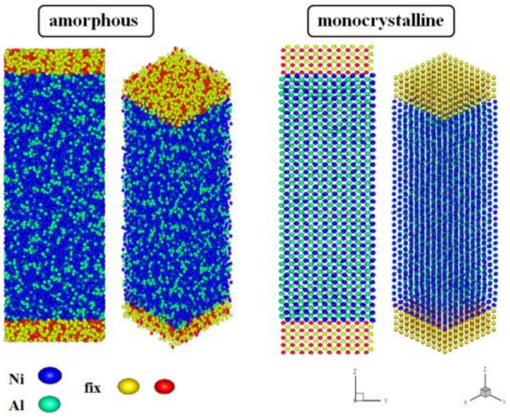

Fig. 5. The configuration of monocrystalline and amorphous Ni-Al nanoalloys at 300 K.

Fig. 6 depicts the relationship between the radial distribution function and the radial separation for the different amorphous Ni–Al nanoalloys at 300 K. After rapid cooing from 1500 K to 300 K, the first peaks of the radial distribution functions of all three amorphous Ni–Al nanoalloys are intensified and sharpened. It can be seen that the location of the first peak is slightly different for the various compositions.

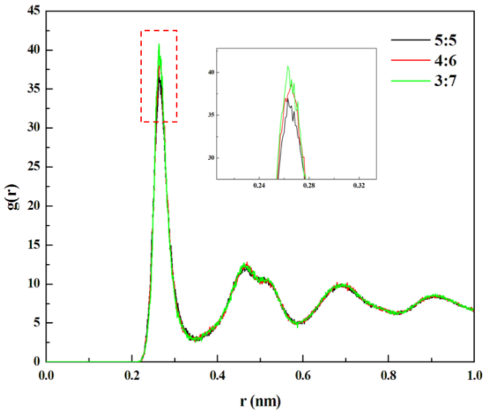

Fig. 6. Comparison of radial distribution functions for different compositions of amorphous Ni-Al nanoalloy at 300 K

Fig. 7 shows the elastic moduli $(C^s)_{ij,kl}$ for the different Ni–Al nanoalloys at 300 K, which were calculated using

$$\delta(\varepsilon_{ij}\varepsilon_{kl}) = \frac{k_b T}{V_0}(C^s)^{-1}_{ij,kl}, \tag{4}$$

where T is the instantaneous temperature, V_0 is the initial volume, k_b is the Boltzmann constant (1.38065×10^{-23} J/K), and ε_{ij} is the strain in the second-order tension. At equilibrium, the elastic moduli of the Ni–Al nanoalloys are varied. For the cases simulated here, the elastic modulus of the Ni–Al nanoalloy with a ratio of 5:5 is the greatest and that of the nanoalloy with a ratio of 3:7 is the smallest because the elastic modulus of Ni is higher than that of Al.

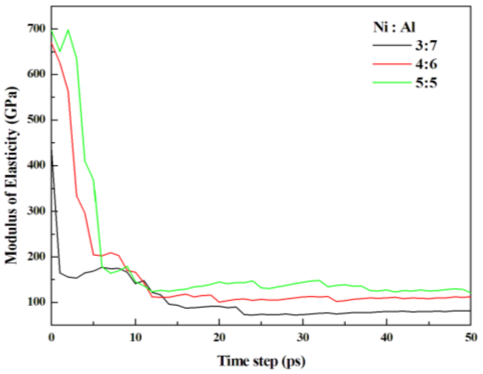

Fig. 7. The variation of the modulus of elasticity with time steps for different compositions of Ni-Al nanoalloy at 300 K

3.3 Necking under uniaxial tension

Snapshots of the slip vector at the critical necking point at 300 K for the Ni–Al nanoalloys with different compositions are depicted in Fig. 8. The slip vector is used as a measure of local plastic deformation and can be found in the neck region. From the figure, it can be seen that the plastic deformation of the amorphous Ni–Al nanoalloy is greater than that of the monocrystalline one. In addition, the plastic deformation of the Ni–Al nanoalloy with a ratio of 3:7 is the greatest. It should be noted that the composition of the amorphous Ni–Al nanoalloy with a ratio of 5:5 was the same as that of the monocrystalline one. Comparing the two cases, it is evident that the monocrystalline Ni–Al nanoalloy experiences more uniform area reduction in the neck region. In contrast, the amorphous Ni–Al nanoalloy with a ratio of 5:5 exhibits a sudden area reduction. This reduction was calculated from the percentage decrease in the cross-sectional area of a tensile test sample caused by necking of the specimen.

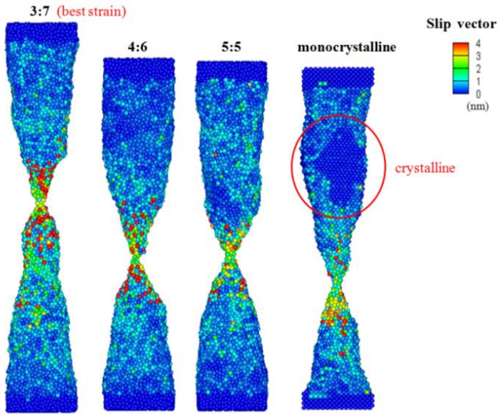

Fig. 8. The critical snapshots of the slip vector for different compositions of Ni-Al nanoalloy during maximum necking at 300 K

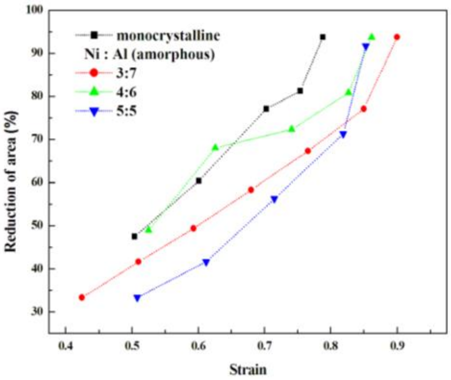

Fig. 9. The reduction of area as a function of strain for different compositions of Ni-Al nanoalloy at 300 K.

Fig. 9 shows the area reduction as a function of strain at 300 K for the Ni–Al nanoalloys with different compositions. The area reduction contributed to the measured ductilities of the metals in a tensile test. As shown in Fig. 9, the area reduction increases with increasing strain. High area reduction indicates significant localized deformation. The area reduction and critical strain in the monocrystalline Ni–Al nanoalloy are 93.35% and 0.77, respectively. The maximum area reductions of the Ni–Al samples with ratios of 3:7, 4:6, and 5:5 are approximately 93.35%, 93.35%, and 91.4%, corresponding to critical strains of 0.91, 0.86, and 0.85, respectively. Comparing the curves of the amorphous Ni–Al nanoalloy with a ratio of 5:5 with those of the monocrystalline one, it is evident that the strain in the monocrystalline Ni–Al nanoalloy is smaller than that in the amorphous one. However, the opposite is true of the area reduction. This difference can be used to explain the fact that the reduction of area of the monocrystalline Ni–Al nanoalloy in the neck region is more uniform than that of the amorphous one, as shown in Fig. 8.

3.4 Effects of equilibrium temperature

Snapshots of the slip vector during necking for an amorphous Ni–Al nanoalloy with a ratio of 3:7 are presented in Fig. 10 at different equilibrium temperatures. The plastic deformation increases with increasing temperature, and the elongation increases dramatically above 500 K, implying that the amorphous Ni–Al nanoalloy with a ratio of 3:7 exhibits high ductility above 500 K. At 700 K, a high-slip-vector region, which is also a high-deformation region, can be found.

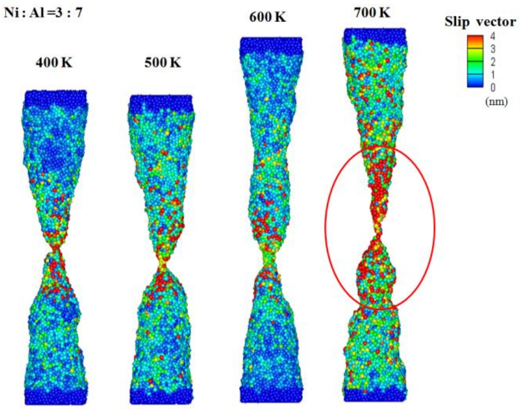

Fig. 10. The snapshots of the slip vector for amorphous Ni-Al nanoalloy with a ratio of 3:7 at different equilibrium temperatures during maximum necking.

Radial distribution function curves for the Ni–Al nanoalloy with a ratio of 3:7, at temperatures of 400–700 K, are shown in Fig. 11. These curves are almost the same at different temperatures. However, the height of the first peak decreases slightly with increasing temperature, indicating that the nanoalloy gradually returns to a steady state due to the thermal effect.

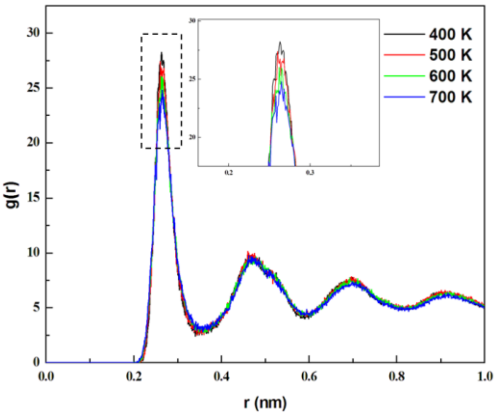

Fig. 11. Comparison of radial distribution functions for Ni-Al nanoalloy with a ratio of 3:7 at different equilibrium temperatures.

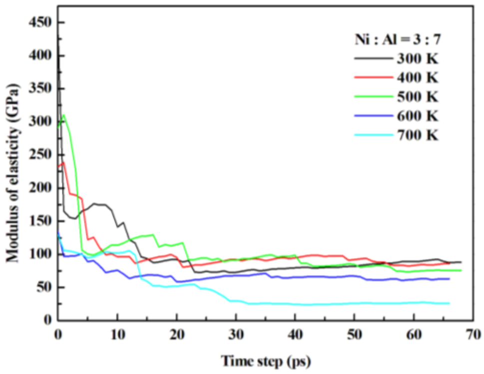

Fig. 12. The variation of modulus of elasticity with time step for the Ni-Al nanoalloy with a ratio of 3:7 at different equilibrium temperatures

The elastic moduli of the Ni–Al nanoalloy with a ratio of 3:7 at different equilibrium temperatures are illustrated in Fig. 12. As time passes, the elastic modulus of the Ni–Al nanoalloy gradually reaches a constant value. After reaching an equilibrium state, the elastic modulus decreases with increasing temperature, indicating that the nanoalloy strength decreases with increasing equilibrium temperature. This behavior is evident because that Ni–Al alloy had a longer atomic distance than the other alloys, leading to weaker metallic bonding at higher temperatures. The simulated results are in agreement with those of the previous study [19].

4. Conclusions

In the research reported herein, the physical and mechanical properties of Ni–Al nanoalloys with different compositions were studied during quenching using MD simulation with a many-body TB potential. The following characteristics were observed in the simulation results:

The radial distribution function of the monocrystalline state had higher peaks and deeper valleys than that of the amorphous state had. The location of the first peak slightly varied for the different compositions. The height of the first peak slightly decreased with increasing equilibrium temperature.

The thermal expansion coefficient of the Ni–Al nanoalloy with a ratio of 5:5 was larger in the liquid state than in the solid phase. After quenching, the phase transformation of the nanoalloy from monocrystalline to amorphous resulted in a volume expansion of approximately 1.5%.

The plastic deformation of the amorphous Ni–Al nanoalloy subjected to a tensile load was larger than that of the monocrystalline one. For the simulated cases, the plastic deformation was the greatest in the Ni–Al nanoalloy with a ratio of 3:7. In the neck region, the area reduction of the monocrystalline Ni–Al nanoalloy with a ratio of 5:5 was more uniform than that of the amorphous one.

The elastic modulus of the amorphous Ni–Al nanoalloy with a ratio of 5:5 was the greatest and that of the nanoalloy with a ratio of 3:7 was the smallest. The elastic modulus of the amorphous Ni–Al nanoalloy with a ratio of 3:7 decreased with increasing temperature once the equilibrium state was reached.

Acknowledgments

The authors wish to thank the Ministry of Science and Technology of Taiwan for providing financial supports for this study under projects MOST 103-2221-E-151 -007 -MY3 and MOST 104-2221-E-168-026.

References

[1] D.B. Miracle, The physics and mechanical properties of NiAl, Acta Metall. Mater. **41,** 649 (1993).

[2] R.D. Noebe, R.R. Bowman, and M.V. Nathal, Int. Mater. Rev. **38**, 193 (1993).

[3] N. Ta, L. Zhang, and Y. Du, Metall. Mater. Transac. A **45A**, 1787 (2014).

[4] A.N. Mansour, A. Dmitrienko, and A.V. Soldatov, Phys. Rev. B **55**, 15531 (1997).

[5] *Intermetallic Compounds: Structural Applications*, vol. 4, J.H. Westbrook, R.L. Fleischer, (Eds.), Wiley, New York, 2000.

[6] J. M. Haile, *Molecular Dynamic Simulation*, Wiley, New York, 1992.

[7] R. Smith (ed.), *Atomic and Ion Collisions in Solids and at Surfaces: Theory, Simulation and Applications,* Cambridge University Press, Cambridge,1997.

[8] T.H. Fang, W.J. Chang, and J.C. Yang, Digest J. Nanomat. Biostruct. **7**, 1811 (2012).

[9] T.H. Fang, W.J. Chang, K.P. Lin, and C. I Weng, Nano **9**, 1450087 (2014).

[10] H. Zong, X. Ding, T. Lookman, J. Li, and J. Sun, Acta Materialia **82**, 295 (2015).

[11] E.G. Noya, C. Rey, and L.J. Gallego, J. Non-Cryst. Solids **298**, 60 (2002).

[12] S. Ozgen and O. Adiguzel, J. Phys. Chem. Solids **65**, 861 (2004).

[13] J. B. Zhu, S. Wang, M. H. Qiao, W. N. Wang, and K. N. Fan, J.Non-Cryst. Solids **353**, 2638 (2007)

[14] S. Kazanc, C. Tatar, Int. J. Solids Struct. **45**, 3282 (2008).

[15] E. V. Levchenko, A. V. Evteev, D. R. Beck, I. V. Belova, and G. E. Murch, Comput. Mater. Sci. **50**, 465 (2010).

[16] J. Zhao, K. Chen, R. Liu, and M. Liang, Wear **311**, 65 (2014).

[17] C. D. Wu, T. H. Fang, P. H. Sung, and Q. C. Hsu, Comput. Mater. Sci. **53**, 321 (2012).

[18] F. Cleri and V. Rosato, Phys. Rev. B **48**, 22 (1993).

[19] H.T. Li, J.T. Guo, K.W. Huai, and H.Q.Ye,, Mater. Sci. Technology **23**, 189 (2007).